Research Square

Preprints are preliminary reports that have not undergone peer review.
They should not be considered conclusive, used to inform clinical practice,
or referenced by the media as validated information.

Multi-omics characterization of PRMT5-associated MYC and proliferative programs in Group 3 medulloblastoma

Dongyang Wang
Beijing Tiantan Hospital, Capital Medical University
Zhaoyang Feng
Beijing Tiantan Hospital, Capital Medical University
Yuyan Liang
Beijing Children's Hospital
Ziwei Wang
BGI Research, Wuhan
Xuan Chen
University of Chinese Academy of Sciences
Kaiwen Deng
Beijing Tiantan Hospital, Capital Medical University
Fei Liu
Beijing Tiantan Hospital, Capital Medical University
Yu Su
Beijing YouAn Hospital
Xi Cheng
Beijing Tiantan Hospital, Capital Medical University
Xiangceng Liu
Beijing Children's Hospital, Capital Medical University
Qiao Yang
Affiliated Women and Children's Hospital of the School of Medicine, University of Electronic Science and Technology of China
Zhiyang Chen
Beijing Tiantan Hospital, Capital Medical University
Junyuan Tian
Beijing Tiantan Hospital, Capital Medical University
Yu Liu
Beijing Children's Hospital, Capital Medical University
Hailong Liu
Beijing Tiantan Hospital, Capital Medical University

Wei Wang
Beijing Children’s Hospital
Tao Jiang
zacharytaojiang@163.com

Beijing Children's Hospital, Capital Medical University

Research Article

Keywords: medulloblastoma, Group 3, PRMT5, MYC, multi-omics, prognosis

Posted Date: November 18th, 2026

DOI: https://doi.org/10.21203/rs.3.rs-11632170/v1

License: This work is licensed under a Creative Commons Attribution 4.0 International License.
Read Full License

Additional Declarations: No competing interests reported.

Multi-omics characterization of PRMT5-associated MYC and proliferative programs in Group 3 medulloblastoma

Dongyang Wang[1,#], Zhaoyang Feng[2,1,#], Yuyan Liang[3,4,#], Ziwei Wang[5,#], Xuan Chen[6], Kaiwen Deng[1,2], Fei Liu[2], Su Yu[7,8], Xi Cheng[2], Xiangcen Liu[10], Qiao Yang[9], Zhiyang Chen[1,2], Junyuan Tian[1,2], Yu Liu[10], Hailong Liu[2,*], Wei Wang[3,4,*], Tao Jiang[10,*]

# Equal contribution. *Corresponding authors: Hailong Liu, Wei Wang, and Tao Jiang.

Affiliations

1. Department of Neurosurgery, Beijing Tiantan Hospital, Capital Medical University, Beijing 100070, China

2. Department of Radiotherapy, Beijing Tiantan Hospital, Capital Medical University, Beijing 100070, China

3. Laboratory of Tumor Immunology, Beijing Pediatric Research Institute, Beijing Children's Hospital, Capital Medical University, National Center for Children's Health, Beijing 100045, China

4. Key Laboratory of Major Diseases in Children, Ministry of Education, Beijing Pediatric Research Institute, Beijing Children's Hospital, Capital Medical University, National Center for Children's Health, Beijing 100045, China

5. BGI Research, Wuhan, China

6. College of Life Sciences, University of Chinese Academy of Sciences, Beijing 100049, China

7. Center of Clinical Epidemiology and Biobank, Beijing Youan Hospital, Capital Medical University, Beijing 100069, China

8. School of Public Health, Capital Medical University, Beijing 100069, China

9. Affiliated Women and Children's Hospital of the School of Medicine, University of Electronic Science and Technology of China, Chengdu, Sichuan 610000, China

10. Department of Neurosurgery, Beijing Children's Hospital, Capital Medical University, Beijing 100045, China

Corresponding Authors

Tao Jiang

Address: Department of Neurosurgery, Beijing Children's Hospital, Capital Medical University, Beijing 100045, China

E-mail: zacharytaojiang@163.com

Wei Wang,

Address: Laboratory of Tumor Immunology, Beijing Pediatric Research Institute, Beijing Children's Hospital, Capital Medical University, National Center for Children's Health, Beijing 100045, China

E-mail: wei860729@163.com

Hailong Liu

Address: Department of Radiotherapy, Beijing Tiantan Hospital, Capital Medical University, Beijing 100070, China

E-mail: liuhailonger@163.com

Running Title

PRMT5-associated programs in Group 3 medulloblastoma

Acknowledgments

We thank the patients and their families for their trust and participation in this study.

Abstract

Background: Group 3 medulloblastoma (G3-MB) carries the worst prognosis, and validated therapeutic targets downstream of MYC remain limited. We investigated PRMT5-associated molecular and clinical features in G3-MB.

Methods and Results: We integrated 763 bulk transcriptomes, approximately 25,000 single-nucleus RNA-seq profiles from 12 G3-MB patients, and 144 paired methylation-expression data. PRMT5 was higher in G3-MB than in SHH tumors and was independently associated with poor overall survival in an institutional validation cohort. Its expression was not associated with copy-number gain, but correlated with promoter hypomethylation and MYC/E2F1/SP1 co-expression. Network analysis placed PRMT5 in a MYC-correlated module enriched for ribosome biogenesis. At single-nucleus resolution, PRMT5-positive tumor cells showed elevated MYC and proliferation programs, although these associations were sensitive to detection threshold and library size. PRMT5-high tumors showed expression of genes linked to PRMT5-inhibitor pathways, DNA damage response, and replication stress. An exploratory seven-gene PRMT5-associated continuous score showed prognostic signal in the training and institutional validation cohorts.

Conclusions: Integrated analyses associate PRMT5 with MYC-linked ribosome biogenesis and proliferative programs in G3-MB. PRMT5 is a candidate prognostic marker, and the PRMT5-MYC-ribosome association is a testable preclinical hypothesis; functional studies are needed to establish therapeutic relevance.

Abbreviations

G3-MB, Group 3 medulloblastoma; snRNA-seq, single-nucleus RNA sequencing; CNV, copy-number variation; GEO, Gene Expression Omnibus; WGCNA, weighted gene co-expression network analysis; GSEA, gene set enrichment analysis; FDR, false discovery rate; HR, hazard ratio; OR, odds ratio; UMAP, uniform manifold approximation and projection; BH, Benjamini-Hochberg.

Keywords

medulloblastoma; Group 3; PRMT5; MYC; multi-omics; prognosis

1. Introduction

Medulloblastoma is the most common malignant pediatric brain tumor, comprising approximately 20% of childhood central nervous system malignancies [1]. Consensus molecular classification defines four subgroups—WNT, SHH, Group 3, and Group 4—with distinct biology and outcomes [2,3].

Group 3 medulloblastoma (G3-MB) carries the worst prognosis, with 5-year overall survival of 50–60%. It is characterized by MYC oncogene activation through genomic amplification, enhancer hijacking, or other mechanisms leading to overexpression [4,5,6]. Direct MYC inhibition remains pharmacologically intractable. No studies have systematically identified and validated pharmacologically tractable downstream targets in the MYC network.

Protein arginine methyltransferase 5 (PRMT5) catalyzes symmetric dimethylation of arginine residues on histones and non-histone substrates. It regulates chromatin remodeling, RNA splicing, ribosome biogenesis, and DNA damage response [7,8]. PRMT5 overexpression drives proliferation in glioblastoma, leukemia, and lung cancer [9,10,11]. MYC transcriptionally activates PRMT5 in several malignancies, establishing a feed-forward ribosome biogenesis loop [12,13].

PRMT5 inhibition has entered early-phase clinical testing in adult myeloid neoplasms with pemrametostat [14], while LLY-283 and EPZ015666 provide preclinical proof-of-concept for PRMT5 inhibition [15,16]. However, PRMT5 has not been characterized through multi-omics integration in medulloblastoma.

Here, we integrate bulk transcriptomic, snRNA-seq, paired methylation-expression, external validation, and spatial transcriptomic data to study PRMT5 in G3-MB. The analysis links PRMT5 overexpression to epigenetic and transcriptional features, identifies a PRMT5-positive proliferative cell state, and supports an exploratory prognostic score with external validation. This study provides computational evidence for PRMT5's association with MYC-driven biology in G3-MB. Experimental validation of these associations and functional testing of PRMT5 inhibitors in preclinical models are required to establish therapeutic potential.

2. Materials and Methods

2.1 Datasets

Bulk transcriptomic data: GSE85217 (n = 763 primary MB) was the discovery/training dataset [3]. The study-design schematic also records a 105-sample matched G3 survival resource. For external validation, we assembled and curated an institutional bulk mRNA cohort of 322 medulloblastoma patients treated at Beijing Tiantan Hospital. After matching expression profiles to clinical annotation, 287 patients were matched and 281 had evaluable survival data. The primary external G3 survival analysis included 68 patients with 28 events. Training and validation cohorts were completely non-overlapping.

Single-nucleus RNA-seq: We generated the snRNA-seq data from 12 treatment-naive G3-MB patients at Beijing Tiantan Hospital. Approximately 25,000 single-nucleus profiles were processed with Seurat v5. SCTransform normalization followed the regularized negative-binomial framework [17], and integration and visualization followed the Seurat workflow [18]. PCA used 30 PCs, followed by UMAP dimensionality reduction and Louvain clustering. Cell types were annotated by canonical markers. Tumor states were assigned using Monocle3 pseudotime and correlation with published developmental programs [19,20].

DNA methylation: GSE85212 and GSE85217 were generated from the same 763-sample primary medulloblastoma resource [3]. We performed specimen-level matching using the shared stable MB_SubtypeStudy_ sample title

recorded in both GEO series matrices. Records without a unique one-to-one match or a Group 3 subtype annotation were excluded, yielding 144 matched G3 samples. The crosswalk records the expression and methylation GEO accessions, shared sample title, molecular subtype, and inclusion status. Four pre-specified CpG probes at the PRMT5 locus were analyzed; their Illumina identifiers, genomic coordinates, and gene-region annotations are reported with the analysis code.

Spatial transcriptomics: GSE252090 was used for spatial niche visualization [21].

2.2 Statistical analysis

Group comparisons: Wilcoxon/Kruskal-Wallis. Correlations: Spearman. Survival: Kaplan-Meier, log-rank, Cox proportional hazards. Multiple testing: Benjamini-Hochberg FDR < 0.05. Differential expression: limma [22]. Network analysis: WGCNA with signed networks [23]. GSEA: fgsea with 10,000 permutations [24]. LASSO Cox: glmnet with 10-fold cross-validation [25].

2.3 Single-nucleus RNA-seq models

PRMT5 positivity was defined as raw count > 0, a binary detection threshold appropriate for moderately expressed genes subject to dropout. Throughout this manuscript, we use 'PRMT5-positive' to denote single nuclei/cells with raw count > 0, and 'PRMT5-high' to denote tumors or patients with elevated PRMT5 expression relative to the cohort distribution.

Pseudotime association was modeled using binomial GLM. Sensitivity analyses varied the PRMT5 detection threshold and model adjustment, including available quality-control and CNV covariates. Program comparisons used cell-level linear models with patient fixed effects. Pseudobulk differential expression used a patient-paired design.

2.4 Target pathway scores

Mean z-scored expression of drug target genes. Scores quantify pathway expression, not empirical sensitivity.

2.5 Risk signature

LASSO Cox on the G3 training cohort used candidate genes from PRMT5, MYC/MYCN, hub genes, ribosome/translation genes, proliferation genes, and DDR/replication markers. Lambda selection identified 7 genes. Validation applied the same coefficients to independently z-scored expression in the external cohort, making the score an exploratory continuum normalized within each cohort.

Ethics approval and informed consent

The study was conducted in accordance with the Declaration of Helsinki and its subsequent amendments. The single-nucleus RNA-sequencing cohort was approved by the Ethics Committee of Beijing Tiantan Hospital, Capital Medical University (Approval No. KY 2019-098-01). Written informed consent was obtained from all participants or their legal guardians before sample collection. Ethical approval was not required for GSE85217, GSE85212, and GSE252090 because these datasets were obtained from public repositories with appropriate data-use agreements.

3. Results

3.1 PRMT5 is elevated in G3-MB and associates with poor survival

We analyzed PRMT5 expression in the GSE85217 cohort (n = 763 medulloblastoma samples) (Fig. 1a). PRMT5 expression was higher in G3-MB than in SHH (BH-adjusted P = 6.5e-4), and G3 also showed a higher median expression than Group 4 (Fig. 1b). Within G3 subtypes, expression was broadly maintained across G3α, G3β, and G3γ (Fig. 1c), indicating a pan-G3 expression feature.

Within G3, PRMT5 and MYC were positively correlated (n = 144, Spearman rho = 0.49, P = 8.7e-10). In G3, the majority of tumors exhibited PRMT5-high/MYC-high co-occurrence (99/144 co-high cases; OR = 7.86, BH-adjusted P = 6.5e-26; Fig. 1d, 1e).

In the external validation cohort with matched expression and survival data, PRMT5-high tumors had reduced overall survival in the full cohort (n = 281, events = 93, HR = 1.60, log-rank P = 0.028; Fig. 1f). Within external G3 tumors, the association was stronger (n = 68, events = 28, HR = 4.22, log-rank P = 3.5e-4; Fig. 1g). Continuous PRMT5 was adverse across clinically, treatment-, and chemotherapy-adjusted sensitivity models (full cohort HR = 1.48-1.53; G3 HR = 2.07-2.22; all P < 0.001; Fig. 1h).

3.2 PRMT5 overexpression associates with promoter hypomethylation and transcription factor co-expression

Having established PRMT5's clinical association with poor survival, we next investigated the regulatory mechanisms underlying its overexpression.

Copy number analysis confirmed that PRMT5 harbors no focal amplification in G3 tumors, in contrast to MYC and MYCN which show significant amplifications. PRMT5 expression showed no correlation with local CNV status, ruling out genomic amplification as the driver.

Using paired methylation and expression data for 144 G3 tumors, we identified PRMT5-region promoter methylation features. Promoter methylation differed significantly across G3 subtypes (Kruskal-Wallis P = 4.57e-9, Fig. 2a, 2b). PRMT5 expression differed across promoter-methylation tertiles (Kruskal-Wallis P = 0.0013), with lower methylation associated with higher expression (Fig. 2c). Continuous promoter methylation correlated negatively with PRMT5 expression (Pearson r = -0.383, P = 2.11e-6; Spearman rho = -0.328, P = 6.15e-5; Fig. 2d).

Among transcription factors with positive PRMT5 co-expression in G3, MYC ranked highest, followed by E2F1 and SP1 (Fig. 2e). MYC ranked in the top 1.1% of all PRMT5-correlated genes.

A composite MYC/E2F1/SP1 TF score correlated with PRMT5 (Pearson r = 0.510, P = 6.72e-11; Spearman rho = 0.434, P = 5.40e-8). After methylation and subtype adjustment, the TF-PRMT5 association remained significant in partial-residual analysis (r = 0.338, P = 3.45e-5; model TF P = 4.18e-5; Fig. 2f). An integrated model showed independent contributions from TF score (coefficient = 0.118, P = 4.18e-5) and promoter methylation (coefficient = -0.0679, P = 0.0159; adjusted R2 = 0.343; Fig. 2g, 2h).

These results represent associative evidence. Causal validation requires ChIP-seq and perturbation experiments. Whether hypomethylation drives or results from PRMT5 expression cannot be determined from correlative data. The integrated model leaves substantial PRMT5 expression variance unexplained, suggesting additional unmeasured contributors.

3.3 PRMT5 defines a co-expression module enriched for ribosome biogenesis and MYC targets

A network connecting PRMT5, hub genes, and MYC targets illustrates convergence onto ribosome biogenesis and cell cycle programs (Fig. 3a).

Differential gene expression analysis between PRMT5-high and PRMT5-low G3 tumors identified thousands of differentially expressed genes (Fig. 3b). Top PRMT5-correlated genes were enriched for nucleotide metabolism, RNA modification, and ribosome biogenesis functions (Fig. 3c).

Gene co-expression network analysis placed PRMT5 in a module showing the strongest MYC correlation (Fig. 3d). Hub genes (highly connected nodes in the co-expression network) were core ribosome biogenesis and translation components (Fig. 3e).

Pathway enrichment showed strong enrichment for cytoplasmic translation, ribosome biogenesis, and cell cycle processes (Fig. 3f, 3g).

Gene set enrichment confirmed MYC_TARGETS_V1 (MSigDB Hallmark gene set) as the top enriched pathway, followed by E2F_TARGETS and G2M_CHECKPOINT (Fig. 3h).

3.4 Single-cell analysis reveals a PRMT5-positive malignant state

Bulk transcriptomic analysis revealed PRMT5's association with ribosome biogenesis pathways. To determine whether this pattern exists at cellular resolution, we analyzed single-nucleus RNA-seq data.

We analyzed snRNA-seq data from 12 treatment-naïve G3-MB patients at Beijing Tiantan Hospital, comprising approximately 25,000 single-nucleus profiles. Five tumor states were identified. Pseudotime analysis (computational ordering of cells along developmental trajectories) reconstructed a developmental trajectory (Fig. 4a).

PRMT5-positive cells comprised a subset of tumor cells (Fig. 4b). PRMT5-positive fractions varied across cell states (Fig. 4c). In continuous pseudotime models, PRMT5 positivity decreased with pseudotime, demonstrating PRMT5 enrichment in less-differentiated cells (Fig. 4e).

PRMT5-positive cells had significantly elevated MYC module scores and proliferation module scores ($P < 0.001$, Fig. 4d). Sensitivity analyses varied the PRMT5 detection threshold and model adjustment. The association was retained in the primary analysis but varied across sensitivity settings (Fig. 4h, 4i), so library size and threshold remain important caveats.

Specificity testing revealed that other proliferation-associated genes with comparable detection rates show equivalent MYC enrichment patterns. This indicates PRMT5-positive cells represent a general transcriptionally active proliferative population. Among co-expressed proliferation genes, PRMT5 is the only member of this proliferative

gene set with clinical-stage small-molecule inhibitors (pemrametostat, onametostat), unlike other proliferation markers such as MKI67 or MCM2.

Patient-level analysis showed consistent patterns across patients (Fig. 4f). Pseudobulk analysis identified G2M_CHECKPOINT, E2F_TARGETS, and MYC_TARGETS_V1 as top pathways in PRMT5-positive cells (Fig. 4g).

3.5 PRMT5-high tumors co-express genes in pathways targeted by clinical inhibitors

Target pathway expression scores in G3 were higher in PRMT5-high tumors for PRMT5-inhibitor proxy genes (delta = 0.540, BH-adjusted P = 4.42e-8), DDR/replication-stress genes (delta = 0.296, BH-adjusted P = 5.69e-5), ATR/CHK1 proxy genes, BET-inhibitor proxy genes, and CDK-inhibitor proxy genes (Fig. 5a-c). The PRMT5-inhibitor proxy score correlated strongly with MYC expression (Spearman rho = 0.88, P < 1e-4, Fig. 5d).

Tumor microenvironment analysis showed no significant PRMT5-high versus low differences in immune signatures or immune-checkpoint expression after correction (Fig. 5e, 5f). These comparisons do not establish overall immune-infiltration level. An evidence-weighted model nominates PRMT5 inhibition for preclinical testing, with combination hypotheses involving ATR/CHK1 and BET inhibitors (Fig. 5g). These scores reflect pathway-level gene expression and should not be interpreted as empirical drug-sensitivity measurements.

3.6 A 7-gene PRMT5-associated continuous score shows exploratory prognostic signal

LASSO Cox modeling in the G3 training cohort selected seven genes: MCM2, RPS25, EIF3H, EIF3M, PRMT5, MYC, and MYCN. Negative coefficients for PRMT5, MYC, and MYCN likely reflect collinearity within the broader PRMT5-MYC co-expression module. Thus, the resulting score is best interpreted as a continuous pathway-level axis capturing ribosome biogenesis, translation, and replication-associated output rather than as a binary clinical classifier.

Cox analysis showed that both PRMT5 expression and the PRMT5-associated continuous score were associated with outcome in G3 medulloblastoma. In the training cohort, the continuous score was associated with increased mortality risk (HR = 1.69 per 1 s.d., P = 2.55e-4). This association was reproduced in the external G3 validation cohort (HR = 2.05 per 1 s.d., P = 6.76e-4) and remained significant after adjustment for clinical covariates (adjusted HR = 2.11 per 1 s.d., P = 5.00e-4; Fig. 6a).

Event-distribution plots showed that deaths were enriched toward higher values of the continuous cohort-normalized score in both the training and external validation cohorts (Fig. 6b). Time-dependent ROC analysis showed moderate discrimination in the training cohort, with 3-, 5-, and 10-year AUCs of 0.755, 0.741, and 0.717, respectively. Similar performance was observed in the external G3 validation cohort, with 3-, 5-, and 10-year AUCs of 0.760, 0.648, and 0.695, respectively (Fig. 6c). Adjusted prediction modeling in the external validation cohort further showed a continuous increase in predicted hazard with increasing risk score (Fig. 6d).

Decision-curve and prediction-curve analyses provided exploratory evidence of 3-year net benefit, but these analyses do not constitute evidence for clinical deployment (Fig. 6e). The median-dichotomized external score was not considered a main positive result, consistent with the statistical penalty and instability introduced by dichotomization.

The risk score correlated with PRMT5 expression and with replication, DNA damage response, and translation/ribosome markers, including MCM2, CHEK1, CDK1, RAD51, RPS25, and EIF3H (Fig. 6f, 6g). These findings confirm that the score captures a PRMT5-MYC-replication co-expression continuum. Of note, PRMT5 expression alone showed numerically strong prognostic performance in the external cohort; therefore, the potential value of the composite score lies primarily in summarizing pathway-level biology rather than replacing PRMT5 as a single-marker readout.

3.7 Spatial architecture of MYC-driven programs in G3-MB

We examined publicly available spatial transcriptomic data from a G3-MB specimen with MYC aberration. The panel did not include PRMT5 transcripts. This analysis characterizes spatial organization of MYC/proliferation programs rather than direct PRMT5 spatial validation.

Spatial analysis revealed distinct localization patterns for MYC/MYCN, proliferation markers, and immune/myeloid genes (Fig. 7a). A composite MYC-proliferation score confirmed spatially contiguous proliferative domains (Fig. 7b), while immune markers occupied distinct regions (Fig. 7c).

Neighborhood-based niche classification identified MYC/proliferative niches spatially segregated from immune/myeloid niches (Fig. 7d). Quantification confirmed functional identity of each spatial domain (Fig. 7e). This spatial segregation is consistent with the lack of PRMT5-stratified immune-signature differences in the bulk analysis.

4. Discussion

We present an integrated multi-omics analysis of PRMT5 in G3-MB, linking its overexpression to regulatory associations, single-nucleus tumor-cell heterogeneity, and prognostic significance.

4.1 PRMT5 regulation

PRMT5 overexpression in G3-MB is not driven by genomic amplification. Instead, it associates with promoter hypomethylation and MYC/E2F1/SP1 co-expression. The TF score remains associated with PRMT5 after adjusting for promoter methylation and subtype. MYC ranks in the top 1.1% of PRMT5-correlated genes.

These findings are consistent with published data showing MYC occupancy at the PRMT5 promoter in other cell types. However, these associations do not establish causality. Direct causal evidence requires ChIP-seq and perturbation in G3-MB models.

4.2 PRMT5-positive cell state

Single-cell analysis identifies a PRMT5-positive state enriched for MYC targets and proliferation. Sensitivity analyses evaluated threshold choice and covariate adjustment while retaining library size and threshold as important caveats.

Specificity testing revealed that other proliferation genes show equivalent MYC enrichment patterns, indicating PRMT5-positive cells represent a general proliferative population rather than a unique state. We prioritize PRMT5 because it has clinical-stage inhibitors (pemrametostat, onametostat), unlike other markers such as MKI67 or MCM2.

This represents an opportunity-driven strategy: targeting an available druggable node within a broader proliferative program.

4.3 Therapeutic hypotheses

PRMT5-high tumors co-express PRMT5-inhibitor target genes alongside DNA damage response and replication stress components. This transcriptomic pattern provides rationale for testing PRMT5 inhibitors, though it does not predict drug sensitivity. The strong correlation with MYC likely reflects general proliferation gene co-expression, requiring functional validation in preclinical models to determine therapeutic potential.

4.4 Prognostic signature

The 7-gene signature shows exploratory prognostic signal in external validation. By "exploratory," we mean the score is cohort-normalized (z-scored independently within each dataset) rather than a locked clinical assay. Translation to clinical use would require prospective validation, standardization to a common reference, and analytical validation in a CLIA-certified laboratory.

The dichotomized version was non-significant in validation, reflecting the statistical penalty of dichotomization. PRMT5 expression alone showed numerically strong discrimination. The composite signature's value may lie in capturing pathway-level biology.

4.5 Limitations

This study has several limitations:

This is a purely computational study. All findings require experimental validation.

Methylation analysis captured only four CpG probes at PRMT5, limiting resolution of epigenetic regulation.

The snRNA-seq cohort lacks matched bulk RNA-seq for the analyzed G3 subset, precluding direct state-outcome correlation.

Spatial data did not include PRMT5 transcripts, limiting validation of PRMT5 spatial patterns.

The external validation cohort is modest (68 G3 patients), and the current matched expression-clinical analysis table does not include directly modelable MYC amplification/cytogenetic status.

The 7-gene score is cohort-normalized, requiring recalibration before clinical application.

4.6 Clinical implications

Prognostic stratification. The signature suggests moderate discrimination within G3-MB but requires prospective validation. The Beijing Tiantan bulk mRNA data were used for external validation; however, the current matched analysis table does not include directly modelable MYC amplification status, so added value beyond MYC amplification could not be tested.

Blood-brain barrier penetration. A critical barrier is drug delivery to the CNS. Current PRMT5 inhibitors (pemrametostat, onametostat) were designed for peripheral malignancies and lack CNS pharmacokinetic profiling in

pediatric brain tumor models. Although high-grade tumors may have regional BBB disruption, no data support adequate whole-tumor penetration. This disruption is often heterogeneous and may not ensure therapeutic drug levels throughout the tumor. Development of CNS-penetrant PRMT5 inhibitors or alternative delivery strategies would strengthen the translational case.

Patient stratification. G3α tumors exhibit the lowest PRMT5 promoter methylation, suggesting potential epigenetic dependence. If hypomethylation drives expression, this subtype may show preferential sensitivity to PRMT5 inhibition. However, this remains speculative. Since PRMT5 overexpression is pan-G3, broader stratification by expression level or the continuous 7-gene score may be more inclusive. PRMT5 inhibition should be considered alongside HDAC, CDK4/6, and BRD4 inhibitors as testable preclinical hypotheses.

5. Conclusions

PRMT5 is preferentially elevated in G3-MB relative to SHH and Group 4 and is associated with poor survival in external validation. Across bulk, snRNA-seq, methylation, and spatial analyses, PRMT5 expression correlates with MYC-linked ribosome biogenesis and proliferation programs. The exploratory 7-gene score supports a prognostic signal, while the PRMT5-MYC-ribosome association provides a focused hypothesis for future preclinical testing in this high-risk pediatric population.

References

[1] Ostrom QT, et al. (2023) CBTRUS statistical report: primary brain and other central nervous system tumors diagnosed in the United States in 2016-2020. Neuro Oncol 25:iv1-iv99. https://doi.org/10.1093/neuonc/noad149

[2] Taylor MD, et al. (2012) Molecular subgroups of medulloblastoma: the current consensus. Acta Neuropathol 123:465-472. https://doi.org/10.1007/s00401-011-0922-z

[3] Cavalli FMG, et al. (2017) Intertumoral heterogeneity within medulloblastoma subgroups. Cancer Cell 31:737-754.e6. https://doi.org/10.1016/j.ccell.2017.05.005

[4] Ramaswamy V, et al. (2016) Risk stratification of childhood medulloblastoma in the molecular era: the current consensus. Acta Neuropathol 131:821-831. https://doi.org/10.1007/s00401-016-1569-6

[5] Northcott PA, et al. (2019) Medulloblastoma. Nat Rev Dis Primers 5:11. https://doi.org/10.1038/s41572-019-0063-6

[6] Northcott PA, et al. (2014) Enhancer hijacking activates GFI1 family oncogenes in medulloblastoma. Nature 511:428-434. https://doi.org/10.1038/nature13379

[7] Stopa N, et al. (2015) The PRMT5 arginine methyltransferase: many roles in development, cancer and beyond. Cell Mol Life Sci 72:2041-2059. https://doi.org/10.1007/s00018-015-1847-9

[8] Blanc RS, Richard S (2017) Arginine methylation: the coming of age. Mol Cell 65:8-24. https://doi.org/10.1016/j.molcel.2016.11.003

[9] Braun CJ, et al. (2017) Coordinated splicing of regulatory detained introns within oncogenic transcripts creates an exploitable vulnerability in malignant glioma. Cancer Cell 32:411-426.e11. https://doi.org/10.1016/j.ccell.2017.08.018

[10] Banasavadi-Siddegowda YK, et al. (2017) PRMT5-PTEN molecular pathway regulates senescence and self-renewal of primary glioblastoma neurosphere cells. Oncogene 36:263-274. https://doi.org/10.1038/onc.2016.199

[11] Xiao W, et al. (2019) Role of protein arginine methyltransferase 5 in human cancers. Biomed Pharmacother 114:108790. https://doi.org/10.1016/j.biopha.2019.108790

[12] Koh CM, et al. (2015) MYC regulates the core pre-mRNA splicing machinery as an essential step in lymphomagenesis. Nature 523:96-100. https://doi.org/10.1038/nature14351

[13] Fong JY, et al. (2019) Therapeutic targeting of RNA splicing catalysis through inhibition of protein arginine methylation. Cancer Cell 36:194-209.e9. https://doi.org/10.1016/j.ccell.2019.07.003

[14] Watts JM, et al. (2024) Phase I/II study of the clinical activity and safety of GSK3326595 in patients with myeloid neoplasms. Ther Adv Hematol 15. https://doi.org/10.1177/20406207241275376

[15] Bonday ZQ, et al. (2018) LLY-283, a potent and selective inhibitor of arginine methyltransferase 5, PRMT5, with antitumor activity. ACS Med Chem Lett 9:612-617. https://doi.org/10.1021/acsmedchemlett.8b00014

[16] Chan-Penebre E, et al. (2015) A selective inhibitor of PRMT5 with in vivo and in vitro potency in MCL models. Nat Chem Biol 11:432-437. https://doi.org/10.1038/nchembio.1810

[17] Hafemeister C, Satija R (2019) Normalization and variance stabilization of single-cell RNA-seq data using regularized negative binomial regression. Genome Biol 20:296. https://doi.org/10.1186/s13059-019-1874-1

[18] Hao Y, et al. (2021) Integrated analysis of multimodal single-cell data. Cell 184:3573-3587.e29. https://doi.org/10.1016/j.cell.2021.04.048

[19] Qiu X, et al. (2017) Reversed graph embedding resolves complex single-cell trajectories. Nat Methods 14:979-982. https://doi.org/10.1038/nmeth.4402

[20] Cao J, et al. (2019) The single-cell transcriptional landscape of mammalian organogenesis. Nature 566:496-502. https://doi.org/10.1038/s41586-019-0969-x

[21] Okonechnikov K, et al. (2025) Oncogene aberrations drive medulloblastoma progression, not initiation. Nature 642:1062-1072. https://doi.org/10.1038/s41586-025-08973-5

[22] Ritchie ME, et al. (2015) limma powers differential expression analyses for RNA-sequencing and microarray studies. Nucleic Acids Res 43:e47. https://doi.org/10.1093/nar/gkv007

[23] Langfelder P, Horvath S (2008) WGCNA: an R package for weighted correlation network analysis. BMC Bioinformatics 9:559. https://doi.org/10.1186/1471-2105-9-559

[24] Korotkevich G, Sukhov V, Sergushichev A (2016) Fast gene set enrichment analysis. bioRxiv:060012. https://doi.org/10.1101/060012

[25] Simon N, Friedman J, Hastie T, Tibshirani R (2011) Regularization paths for Cox's proportional hazards model via coordinate descent. J Stat Softw 39:1-13. https://doi.org/10.18637/jss.v039.i05

Statements and Declarations

Funding

This work was supported by the National Natural Science Foundation of China (Grant Nos. 82273343, 82172608).

Competing interests

The authors report there are no competing interests to declare.

Author contributions

Conceptualization: Dongyang Wang, Zhaoyang Feng, Yuyan Liang, Ziwei Wang, Tao Jiang, Wei Wang, Hailong Liu. Data curation: Dongyang Wang, Zhaoyang Feng, Yuyan Liang, Ziwei Wang, Xuan Chen, Fei Liu, Kaiwen Deng. Formal analysis: Dongyang Wang, Zhaoyang Feng, Yuyan Liang, Ziwei Wang, Xuan Chen, Wei Wang, Hailong Liu. Funding acquisition: Tao Jiang, Wei Wang, Hailong Liu. Investigation: Dongyang Wang, Ziwei Wang, Xuan Chen, Su Yu, Yuyan Liang, Xi Cheng. Methodology: Dongyang Wang, Zhaoyang Feng, Yuyan Liang, Ziwei Wang, Xuan Chen, Tao Jiang, Wei Wang, Hailong Liu. Project administration: Fei Liu, Zhaoyang Feng, Kaiwen Deng. Resources: Su Yu, Yuyan Liang, Xi Cheng. Supervision: Tao Jiang, Wei Wang, Hailong Liu. Visualization: Dongyang Wang, Zhaoyang Feng, Yuyan Liang, Ziwei Wang, Xuan Chen. Writing - original draft: Dongyang Wang, Zhaoyang Feng, Yuyan Liang, Ziwei Wang, Xuan Chen. Writing - review and editing: All authors.

Ethics approval

The single-nucleus RNA-sequencing cohort was approved by the Ethics Committee of Beijing Tiantan Hospital, Capital Medical University (Approval No. KY 2019-098-01). Ethical approval was not required for the cited public GEO datasets, which were obtained with appropriate data-use agreements.

Informed consent

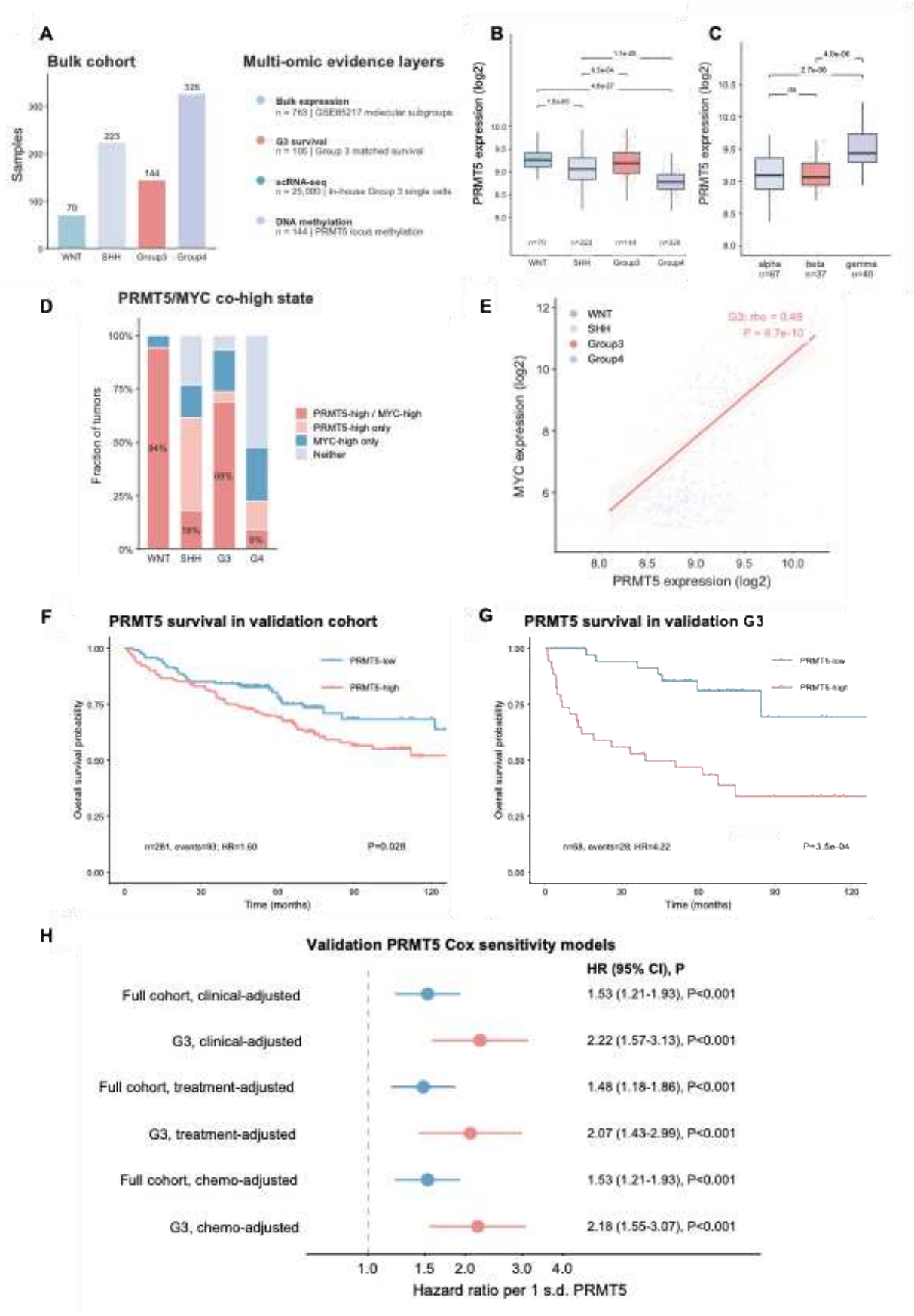
Written informed consent was obtained from all participants or their legal guardians before sample collection.

Data availability

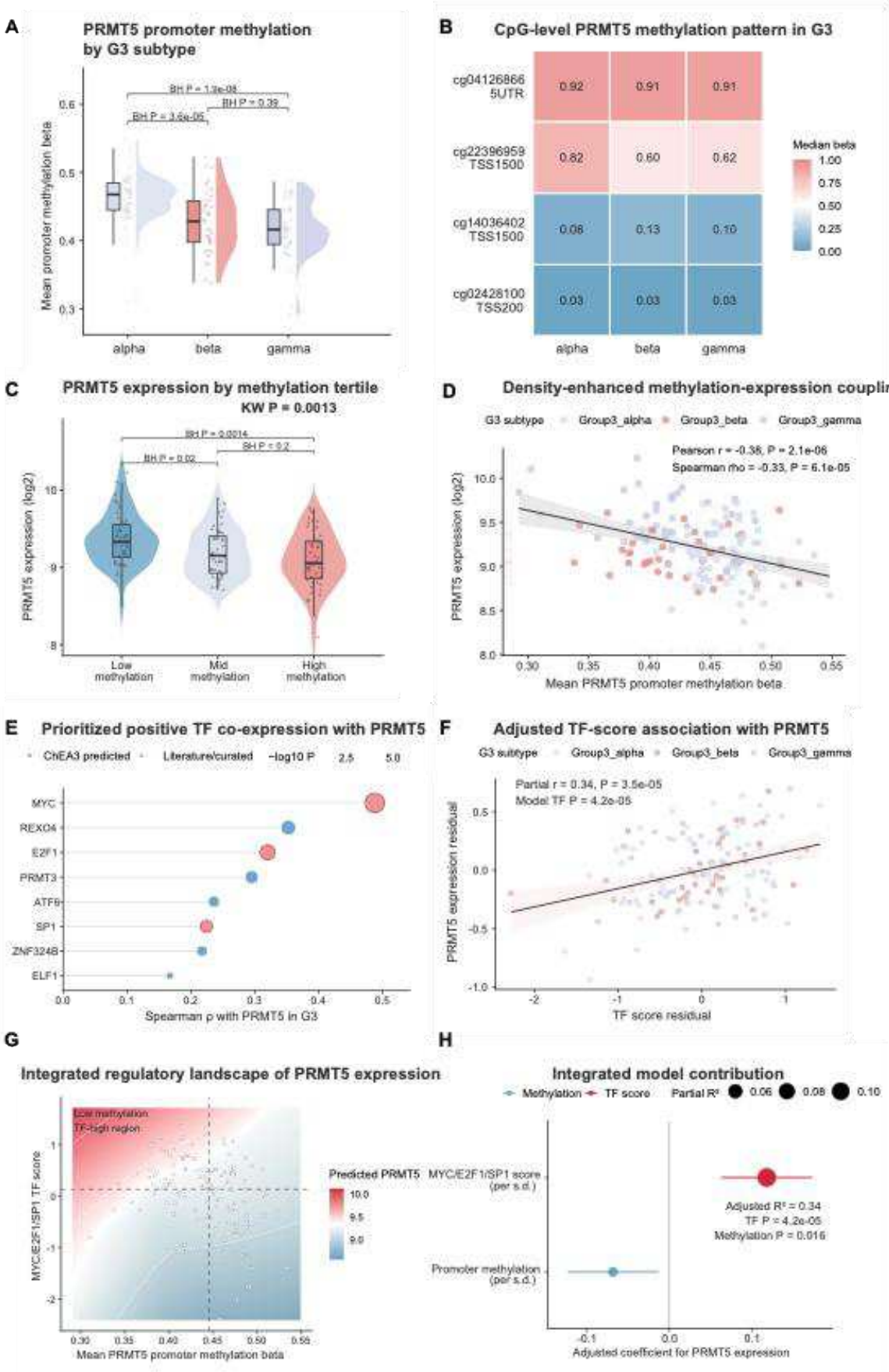
Public datasets are available from the Gene Expression Omnibus (GEO) under accession numbers GSE85217, GSE85212, and GSE252090. The Beijing Tiantan Hospital validation cohort and in-house single-nucleus RNA-sequencing data are not publicly deposited because access is governed by participant consent and institutional requirements. These materials can be provided to qualified reviewers under controlled access where permitted and will be released according to consent and institutional requirements upon acceptance.

Generative AI statement

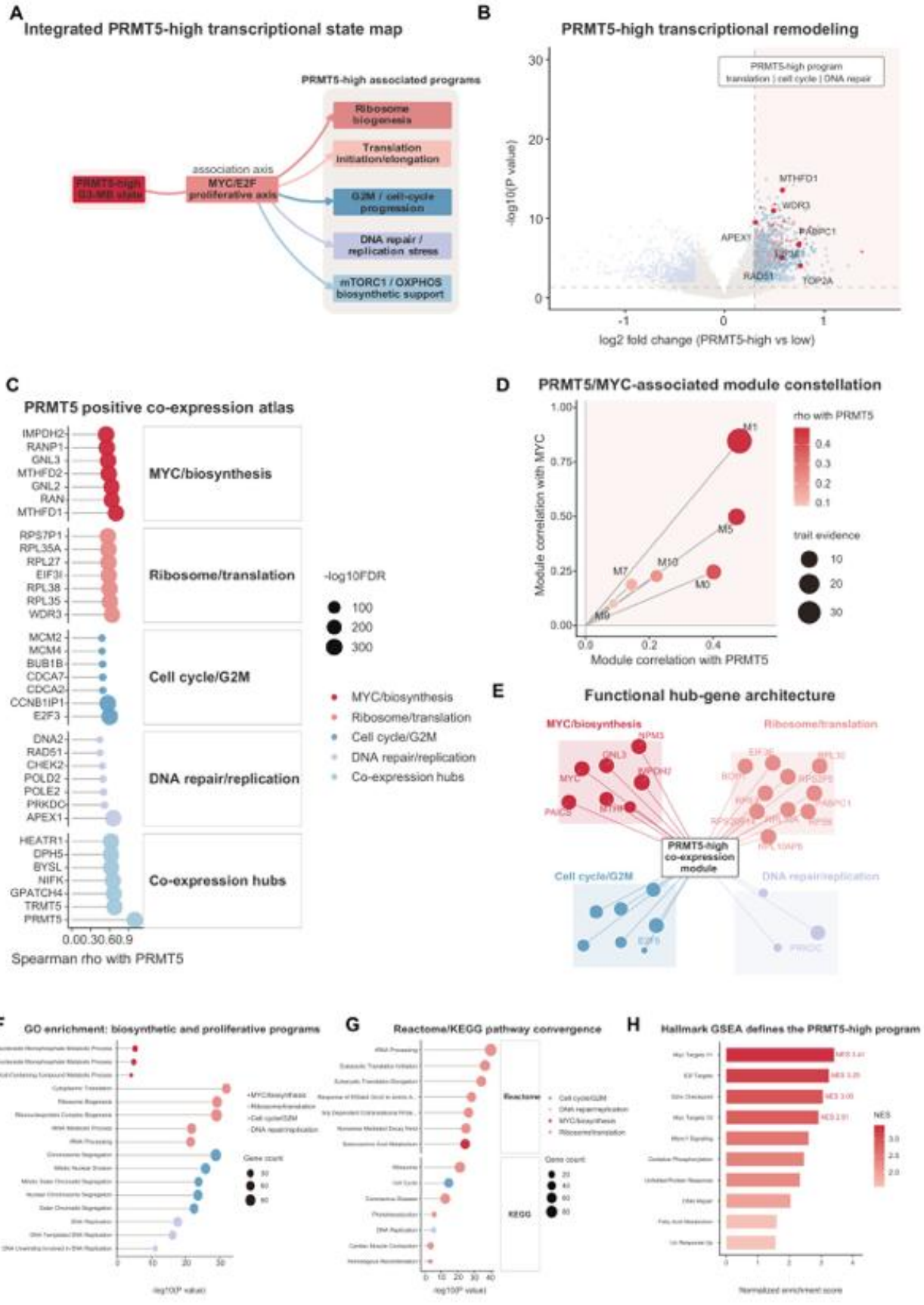
Generative AI was used solely for language and formatting assistance during manuscript preparation. All authors reviewed and verified the final manuscript and remain responsible for its scientific content.


A
Bulk cohort
Samples
70
223
144
325
WNT
SHH
Group3
Group4
Multi-omic evidence layers
Bulk expression
n = 763 | GSE85217 molecular subgroups
G3 survival
n = 105 | Group 3 matched survival
scRNA-seq
n = 25,000 | In-house Group 3 single cells
DNA methylation
n = 144 | PRMT5 locus methylation
B
PRMT5 expression (log2)
C
PRMT5 expression (log2)
alpha
beta
gamma
D
PRMT5/MYC co-high state
Fraction of tumors
PRMT5-high / MYC-high
PRMT5-high only
MYC-high only
Neither
94%
38%
69%
9%
G3
G4
E
WNT
SHH
Group3
Group4
MYC expression (log2)
PRMT5 expression (log2)
F
PRMT5 survival in validation cohort
PRMT5-low
PRMT5-high
Overall survival probability
n=281, events=93; HR=1.60
P=0.028
Time (months)
G
PRMT5 survival in validation G3
PRMT5-low
PRMT5-high
Overall survival probability
n=68, events=28; HR=4.22
P=3.5e-04
Time (months)
H
Validation PRMT5 Cox sensitivity models
HR (95% CI), P
Full cohort, clinical-adjusted
1.53 (1.21-1.93), P<0.001
G3, clinical-adjusted
2.22 (1.57-3.13), P<0.001
Full cohort, treatment-adjusted
1.48 (1.18-1.86), P<0.001
G3, treatment-adjusted
2.07 (1.43-2.99), P<0.001
Full cohort, chemo-adjusted
1.53 (1.21-1.93), P<0.001
G3, chemo-adjusted
2.18 (1.55-3.07), P<0.001
1.0
1.5
2.0
3.0
4.0
Hazard ratio per 1 s.d. PRMT5

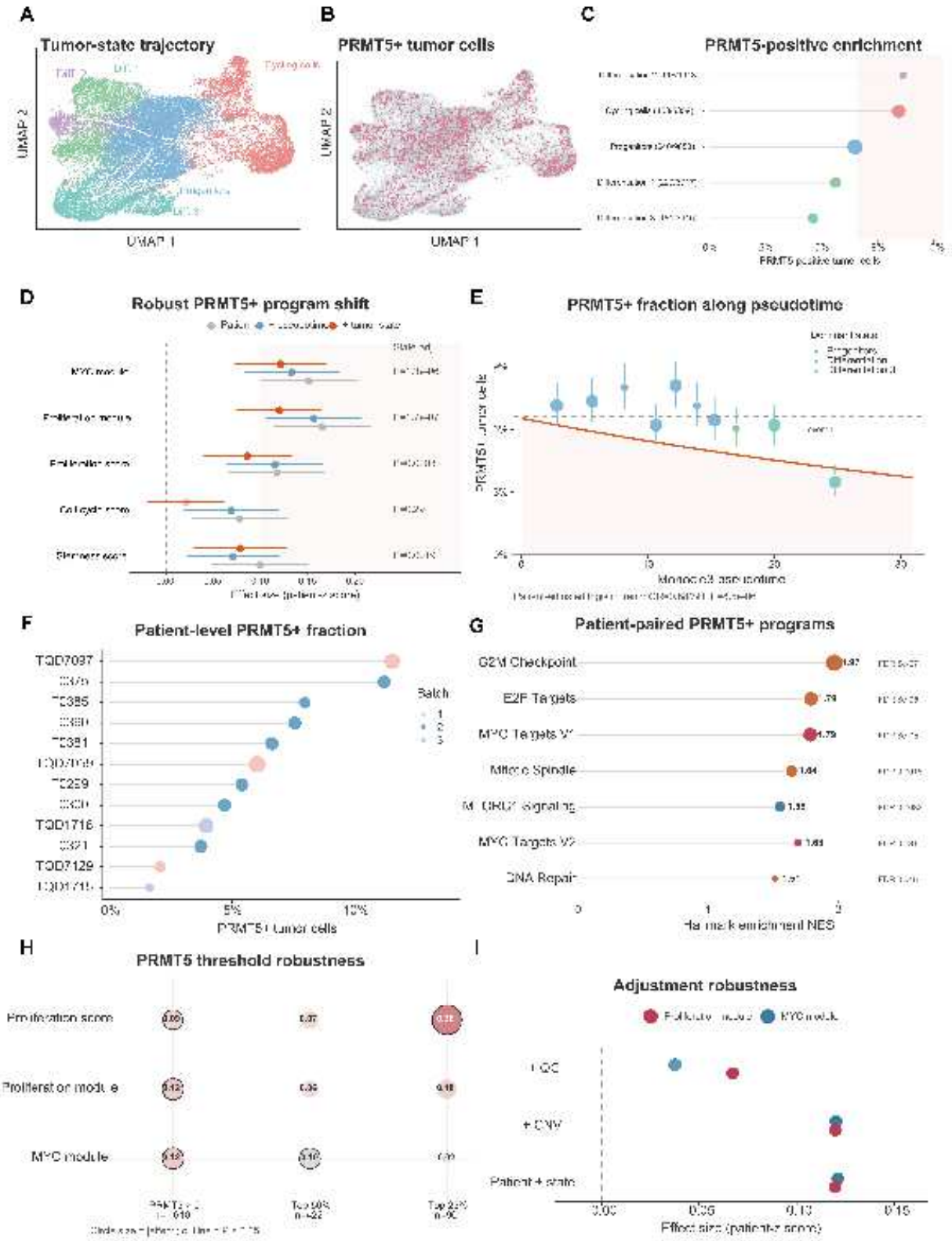
395


A
PRMT5 promoter methylation by G3 subtype
BH P = 1.3e-08
BH P = 0.39
BH P = 3.6e-05
Mean promoter methylation beta
alpha
beta
gamma
B
CpG-level PRMT5 methylation pattern in G3
cg04126866 5UTR
cg22396959 TSS1500
cg14036402 TSS1500
cg02428100 TSS200
0.92
0.91
0.91
0.82
0.60
0.62
0.08
0.13
0.10
0.03
0.03
0.03
Median beta
1.00
0.75
0.50
0.25
0.00
C
PRMT5 expression by methylation tertile
KW P = 0.0013
BH P = 0.0014
BH P = 0.2
BH P = 0.02
PRMT5 expression (log2)
Low methylation
Mid methylation
High methylation
D
Density-enhanced methylation-expression coupling
G3 subtype
Group3_alpha
Group3_beta
Group3_gamma
Pearson r = -0.38, P = 2.1e-06
Spearman rho = -0.33, P = 6.1e-05
PRMT5 expression (log2)
Mean PRMT5 promoter methylation beta
E
Prioritized positive TF co-expression with PRMT5
ChEA3 predicted
Literature/curated
−log10 P
MYC
REXO4
E2F1
PRMT3
ATF6
SP1
ZNF324B
ELF1
Spearman ρ with PRMT5 in G3
F
Adjusted TF-score association with PRMT5
G3 subtype
Group3_alpha
Group3_beta
Group3_gamma
Partial r = 0.34, P = 3.5e-05
Model TF P = 4.2e-05
PRMT5 expression residual
TF score residual
G
Integrated regulatory landscape of PRMT5 expression
Low methylation
TF-high region
MYC/E2F1/SP1 TF score
Predicted PRMT5
Mean PRMT5 promoter methylation beta
H
Integrated model contribution
Methylation
TF score
Partial R²
0.06
0.08
0.10
MYC/E2F1/SP1 score (per s.d.)
Promoter methylation (per s.d.)
Adjusted R² = 0.34
TF P = 4.2e-05
Methylation P = 0.016
Adjusted coefficient for PRMT5 expression

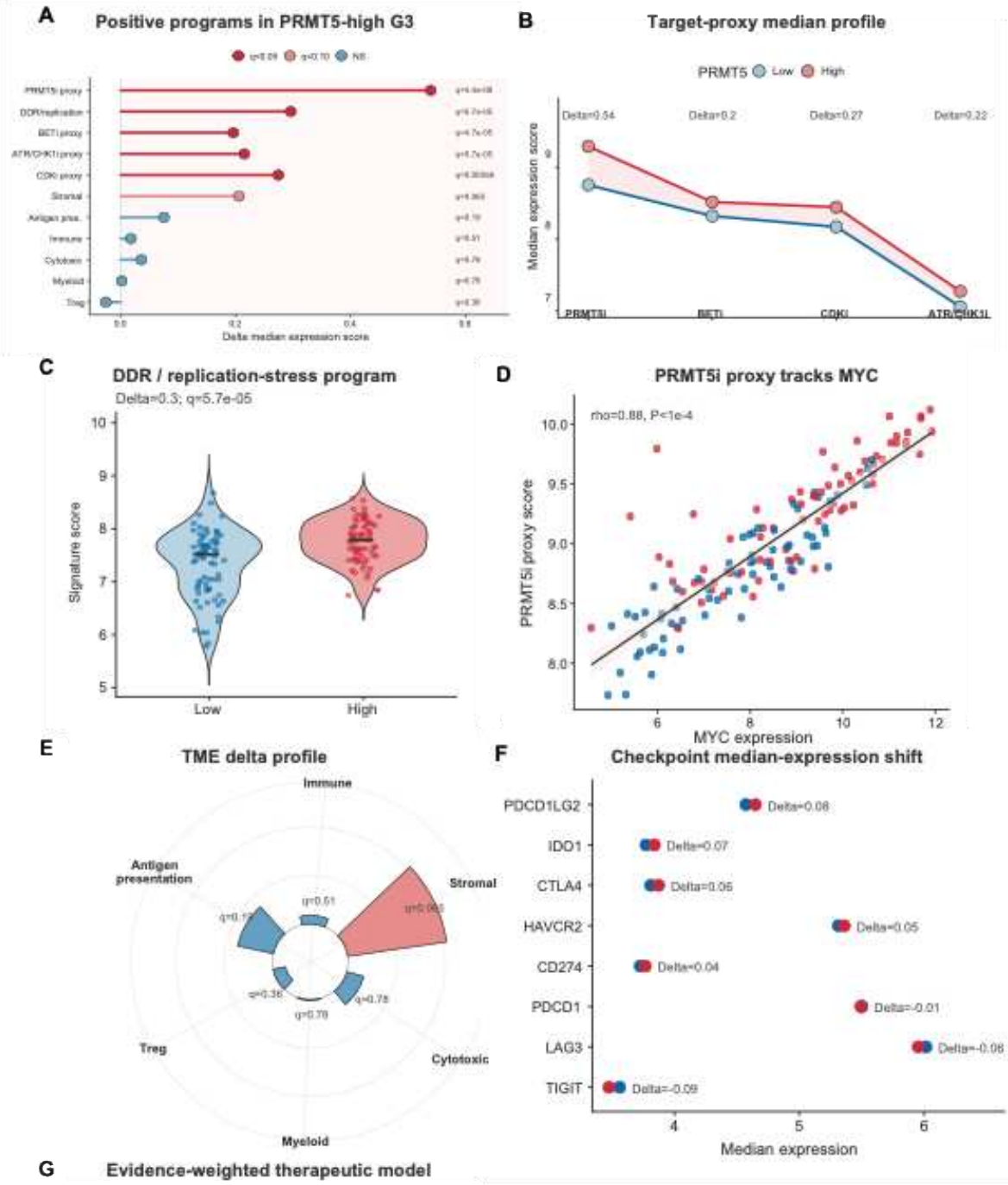
396


A
Integrated PRMT5-high transcriptional state map
PRMT5-high associated programs
PRMT5-high G2/M/E state
association axis
MYC/E2F proliferative axis
Ribosome biogenesis
Translation initiation/elongation
G2M / cell-cycle progression
DNA repair / replication stress
mTORC1 / OXPHOS biosynthetic support
B
PRMT5-high transcriptional remodeling
PRMT5-high program
translation | cell cycle | DNA repair
-log10(P value)
log2 fold change (PRMT5-high vs low)
MTHFD1
WDR3
APEX1
RAD51
TOP2A
C
PRMT5 positive co-expression atlas
IMPDH2
RANP1
GNL3
MTHFD2
GNL2
RAN
MTHFD1
MYC/biosynthesis
RPS7P1
RPL35A
RPL27
EIF3I
RPL38
RPL35
WDR3
Ribosome/translation
MCM2
MCM4
BUB1B
CDCA7
CDCA2
CCNB1IP1
E2F3
Cell cycle/G2M
DNA2
RAD51
CHEK2
POLD2
POLE2
PRKDC
APEX1
DNA repair/replication
HEATR1
DPH5
BYSL
NIFK
GPATCH4
TRMT5
PRMT5
Co-expression hubs
Spearman rho with PRMT5
-log10FDR
MYC/biosynthesis
Ribosome/translation
Cell cycle/G2M
DNA repair/replication
Co-expression hubs
D
PRMT5/MYC-associated module constellation
Module correlation with MYC
Module correlation with PRMT5
rho with PRMT5
trait evidence
E
Functional hub-gene architecture
MYC/biosynthesis
Ribosome/translation
Cell cycle/G2M
DNA repair/replication
PRMT5-high co-expression module
F
GO enrichment: biosynthetic and proliferative programs
G
Reactome/KEGG pathway convergence
Reactome
KEGG
H
Hallmark GSEA defines the PRMT5-high program
NES

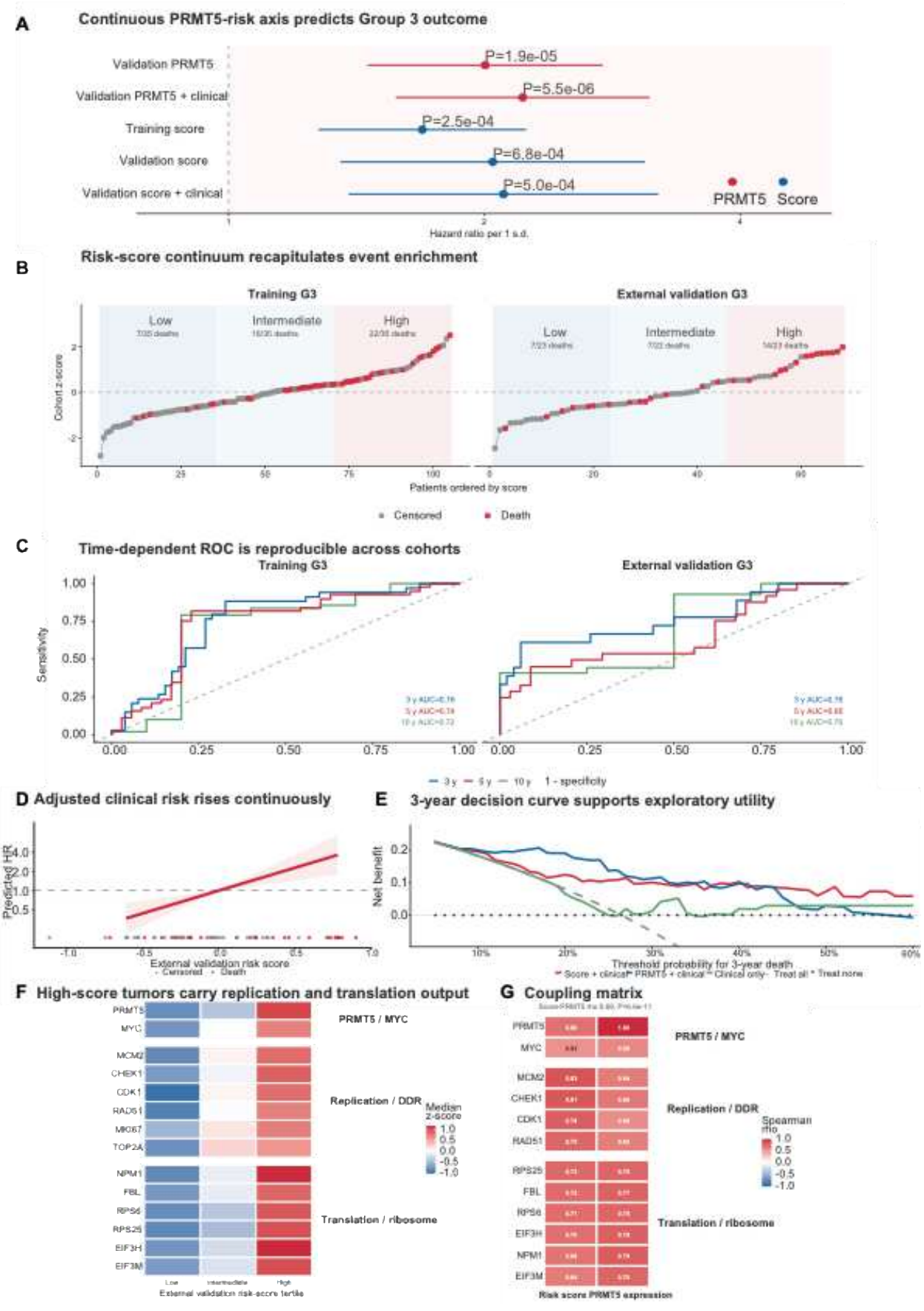
397

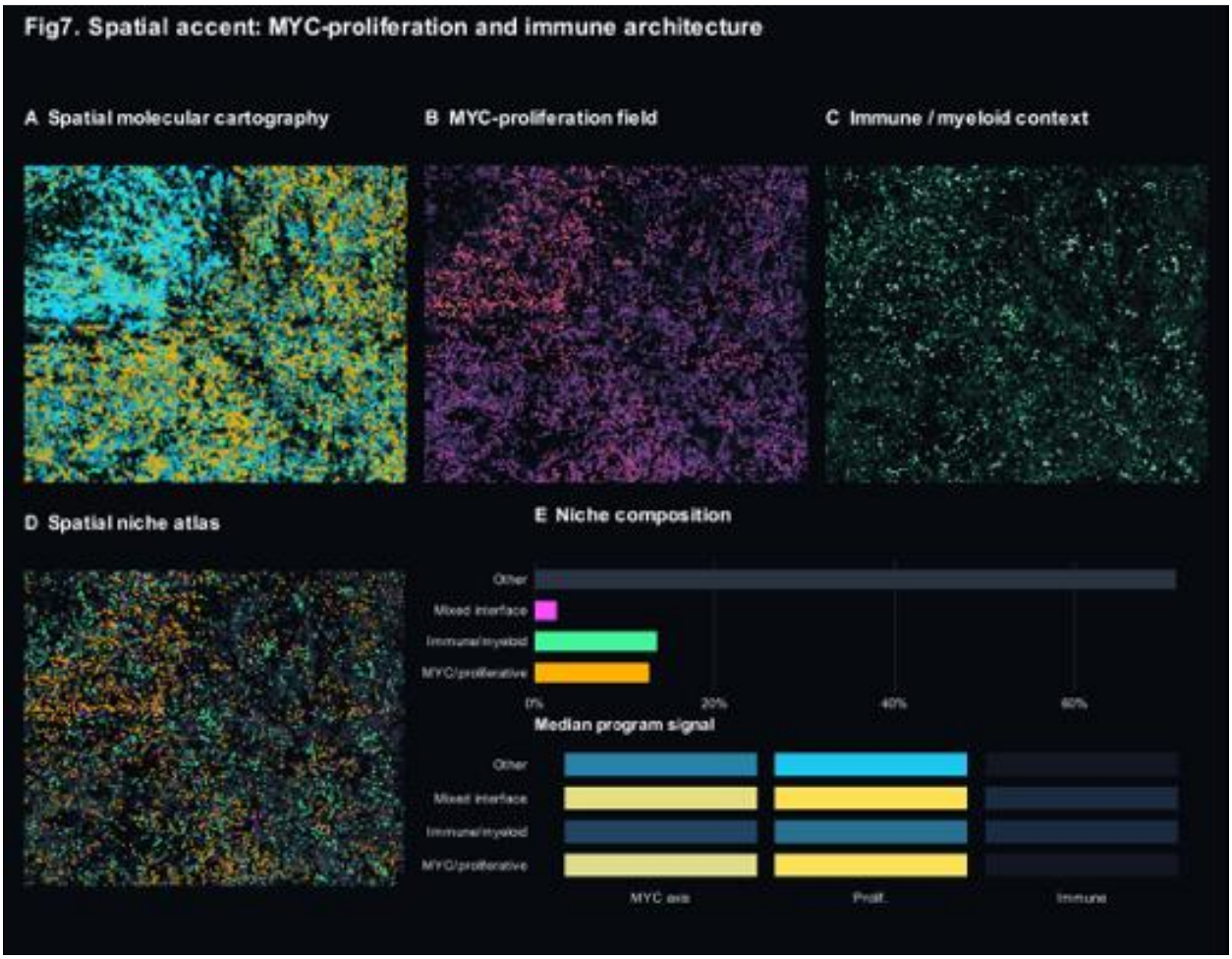

A
Tumor-state trajectory
UMAP 2
UMAP 1
B
PRMT5+ tumor cells
UMAP 2
UMAP 1
C
PRMT5-positive enrichment
D
Robust PRMT5+ program shift
E
PRMT5+ fraction along pseudotime
F
Patient-level PRMT5+ fraction
Batch
PRMT5+ tumor cells
G
Patient-paired PRMT5+ programs
G2M Checkpoint
E2F Targets
MYC Targets V1
Mitotic Spindle
MYC Targets V2
DNA Repair
Hallmark enrichment NES
H
PRMT5 threshold robustness
Proliferation score
Proliferator module
MYC module
I
Adjustment robustness
+ QC
+ CNV
Patient + state
Effect size (patient+ score)

398


A
Positive programs in PRMT5-high G3
Delta median expression score
B
Target-proxy median profile
PRMT5 Low High
Median expression score
PRMT5i
BETi
CDKi
C
DDR / replication-stress program
Delta=0.3; q=5.7e-05
Signature score
Low
High
D
PRMT5i proxy tracks MYC
rho=0.88, P<1e-4
PRMT5i proxy score
MYC expression
E
TME delta profile
Immune
Stromal
Cytotoxic
Myeloid
Treg
Antigen presentation
F
Checkpoint median-expression shift
PDCD1LG2
IDO1
CTLA4
HAVCR2
CD274
PDCD1
LAG3
TIGIT
Median expression
G
Evidence-weighted therapeutic model
PRMT5-high G3 tumor
MYC-coupled PRMT5i proxy
Therapy-proxy classes
Combination hypotheses
DDR / replication stress
Immune context modest

399


A
Continuous PRMT5-risk axis predicts Group 3 outcome
Validation PRMT5
Validation PRMT5 + clinical
Training score
Validation score
Validation score + clinical
P=1.9e-05
P=5.5e-06
P=2.5e-04
P=6.8e-04
P=5.0e-04
PRMT5
Score
Hazard ratio per 1 s.d.
B
Risk-score continuum recapitulates event enrichment
Training G3
External validation G3
Low
Intermediate
High
Cohort z-score
Patients ordered by score
Censored
Death
C
Time-dependent ROC is reproducible across cohorts
Training G3
External validation G3
Sensitivity
1 - specificity
3 y
5 y
10 y
D Adjusted clinical risk rises continuously
Predicted HR
External validation risk score
E 3-year decision curve supports exploratory utility
Net benefit
Threshold probability for 3-year death
F High-score tumors carry replication and translation output
PRMT5
MYC
MCM2
CHEK1
CDK1
RAD51
MKI67
TOP2A
NPM1
FBL
RPS6
RPS26
EIF3H
EIF3M
PRMT5 / MYC
Replication / DDR
Translation / ribosome
Median z-score
External validation risk-score tertile
G Coupling matrix
Spearman rho
Risk score PRMT5 expression



401

402 Figure captions

403 **Fig. 1 PRMT5 expression and clinical association in medulloblastoma.**

404 (a) Study design and cohort overview integrating bulk transcriptomic, DNA methylation (n = 144; PRMT5 locus
405 methylation), snRNA-seq, a matched G3 survival resource (n = 105), spatial transcriptomic, and external validation
406 resources. (b) PRMT5 expression across molecular subgroups in GSE85217. Displayed pairwise BH-adjusted
407 comparisons were WNT versus SHH (P = 1.5e-5), WNT versus Group 4 (P = 4.8e-27), SHH versus Group 3 (P =
408 6.5e-4), and SHH versus Group 4 (P = 1.1e-20); the G3 versus WNT comparison was not significant (P = 0.16). (c)
409 PRMT5 expression across G3 molecular subtypes. (d) PRMT5/MYC co-high status across medulloblastoma
410 subgroups; G3 tumors showed 99/144 co-high cases (OR = 7.86, BH-adjusted P = 6.5e-26). (e) PRMT5-MYC
411 correlation within G3 tumors (n = 144, Spearman rho = 0.49, P = 8.7e-10). (f) Kaplan-Meier analysis in the external
412 full cohort showed adverse overall survival for PRMT5-high tumors (n = 281, events = 93, HR = 1.60, log-rank P =
413 0.028). (g) The association was stronger within external G3 tumors (n = 68, events = 28, HR = 4.22, log-rank P =
414 3.5e-4). (h) Multivariable Cox sensitivity models support PRMT5 as an adverse marker in external validation.

415 **Fig. 2 Epigenetic and transcriptional associations of PRMT5 in Group 3 medulloblastoma.**

(a, b) PRMT5-region promoter methylation patterns across G3 subtypes using paired GSE85212 methylation beta values and GSE85217 expression/subtype metadata (n = 144); promoter methylation differed across G3 subtypes (Kruskal-Wallis P = 4.57e-9). (c) PRMT5 expression differed across promoter methylation tertiles (Kruskal-Wallis P = 0.0013), with lower methylation associated with higher expression. (d) Continuous promoter methylation-expression analysis showed an inverse association (Pearson r = -0.383, P = 2.11e-6; Spearman rho = -0.328, P = 6.15e-5). (e) Positive PRMT5 co-expression prioritized MYC, E2F1, SP1, and additional transcription-factor candidates. (f) A MYC/E2F1/SP1 transcription-factor score remained associated with PRMT5 after promoter methylation and subtype adjustment (partial-residual Pearson r = 0.338, P = 3.45e-5; model P = 4.18e-5). (g, h) Integrated modeling showed independent contributions from TF score (coefficient = 0.118, P = 4.18e-5) and promoter methylation (coefficient = -0.0679, P = 0.0159; adjusted R2 = 0.343). These analyses are associative and do not establish causal regulation.

Fig. 3 PRMT5-high G3 tumors show translation, ribosome biogenesis, and MYC/proliferation enrichment.

(a) Network summary links PRMT5, hub genes, and MYC targets as co-expression associations rather than direct regulatory proof. (b) Differential expression between PRMT5-high and PRMT5-low G3 tumors identified 4,099 FDR-significant genes. (c) Top PRMT5-correlated genes included MTHFD1, TRMT5, GPATCH4, APEX1, NIFK, WDR3, RAN, GNL2, and BYSL, supporting nucleotide metabolism, RNA modification, and ribosome-biogenesis biology. (d) WGCNA module-trait analysis placed PRMT5 in the module most strongly associated with MYC. (e) Hub-gene network visualization highlights ribosome biogenesis and translation components as module hubs. (f, g) GO, Reactome, and KEGG enrichment supported cytoplasmic translation, rRNA processing, ribosome biogenesis, cell cycle, and DNA replication. (h) Hallmark GSEA identified MYC_TARGETS_V1 as the top enriched pathway (NES = 3.41, FDR = 5.0e-49), followed by E2F and G2M programs.

Fig. 4 Single-nucleus analysis identifies PRMT5-positive G3 tumor cells enriched for MYC/proliferation programs.

(a) UMAP and pseudotime structure of snRNA-seq data from 12 treatment-naïve G3-MB patients at Beijing Tiantan Hospital, comprising approximately 25,000 single-nucleus profiles. (b) PRMT5-positive tumor cells were defined by raw count > 0 and represented 1,610/24,387 tumor cells (6.6%). (c) PRMT5-positive fractions varied across tumor states, with higher fractions in cycling and differentiation-associated tumor states. (d) PRMT5-positive cells showed higher MYC and proliferation program scores after patient/state adjustment (MYC beta = 0.121, P = 1.27e-6; proliferation beta = 0.120, P = 1.67e-7). (e) PRMT5-positive fraction decreased along pseudotime, supporting enrichment in less-differentiated regions of the trajectory. (f) Patient-level PRMT5-positive fractions showed reproducible but heterogeneous detection across patients. (g) Pseudobulk pathway analysis identified G2M_CHECKPOINT, E2F_TARGETS, and MYC_TARGETS_V1 among the top PRMT5-positive-cell pathways. (h, i) Threshold and adjustment-robustness analyses supported the association with proliferation/MYC programs while confirming that library size and threshold choice remain important caveats.

Fig. 5 PRMT5-high tumors show expression-based therapeutic-prioritization signals.

(a-c) Target pathway scores were higher in PRMT5-high G3 tumors for PRMT5-inhibitor proxy genes (delta = 0.540, BH-adjusted P = 4.42e-8), DDR/replication-stress genes (delta = 0.296, BH-adjusted P = 5.69e-5), ATR/CHK1 proxy genes, BET-inhibitor proxy genes, and CDK-inhibitor proxy genes. (d) The PRMT5-inhibitor proxy score correlated

strongly with MYC expression (Spearman rho = 0.88, P < 1e-4). (e, f) Immune, cytotoxic, myeloid, Treg, and checkpoint-related expression signatures showed no significant PRMT5-high versus low differences after correction; these comparisons do not establish overall immune-infiltration level. (g) Evidence-weighted prioritization nominates PRMT5 inhibition and combination hypotheses involving ATR/CHK1 and BET inhibition. These panels are expression proxies and should not be interpreted as drug-sensitivity or treatment-response measurements.

Fig. 6 Exploratory PRMT5-associated continuous prognostic score.

The score was constructed from seven genes selected in the G3 training cohort: MCM2, RPS25, EIF3H, EIF3M, PRMT5, MYC, and MYCN. (a) Cox models show that PRMT5 expression and the PRMT5-associated continuous score are associated with outcome in Group 3 medulloblastoma, including after adjustment for clinical covariates in the external validation cohort. Points indicate hazard ratios per 1 standard deviation, and horizontal bars indicate 95% confidence intervals. (b) Event distributions in the training and external validation G3 cohorts show the risk score as a continuous cohort-normalized variable, with deaths enriched toward higher scores. (c) Time-dependent ROC analysis showed moderate discrimination in the training cohort, with 3/5/10-year AUCs of 0.755/0.741/0.717, and in the external G3 validation cohort, with 3/5/10-year AUCs of 0.760/0.648/0.695. (d) Adjusted prediction modeling in the external validation cohort showed a continuous increase in predicted hazard with increasing risk score. (e) Three-year decision-curve analysis provided exploratory net-benefit evidence but does not constitute clinical deployment evidence. (f) High-score external validation tumors showed higher expression of PRMT5/MYC, replication/DNA damage response, and translation/ribosome markers. (g) Correlation analysis confirmed coupling between the risk score, PRMT5 expression, and replication/DDR/translation markers, supporting a PRMT5-MYC-replication co-expression continuum. The median-dichotomized external score was not considered a main positive result.

Fig. 7 Spatial organization of MYC/proliferation and immune/myeloid programs in G3 medulloblastoma.

(a) Spatial transcriptomic visualization of a public G3-MB specimen with MYC aberration; the measured panel did not include PRMT5 transcripts. (b) Composite MYC-proliferation scoring identified spatially contiguous proliferative domains. (c) Immune/myeloid markers occupied distinct spatial regions. (d) Neighborhood-based niche classification separated MYC/proliferative niches from immune/myeloid niches. (e) Quantification showed MYC/proliferative niches in 1,926 spots (12.7%), immune/myeloid niches in 2,055 spots (13.6%), mixed-interface niches in 371 spots (2.45%), and other regions in 10,768 spots (71.2%). This analysis supports spatial organization of MYC/proliferation programs but does not directly validate PRMT5 spatial localization.